ECCOMAS MSF 2017 THEMATIC CONFERENCE
20-22 SEPTEMBER 2017, LJUBLJANA, SLOVENIA

AIRFOIL CATALOGUE FOR WIND TURBINE BLADES WITH OPENFOAM

LORENZO DONISI [1], FELIX SORRIBES PALMER* [2], SANTIAGO PINDADO [2], ANTONIO FIGUEROA [2], SEBASTIAN FRANCHINI [2], MIKEL OGUETA-GUTIERREZ [2], JAVIER PEREZ-ALVAREZ [2] AND OMAR GOMEZ-ORTEGA [2]

[1] Università di Napoli Federico II
[2] Instituto de Microgravedad 'Ignacio Da Riva', Universidad Politécnica de Madrid, felix.sorribes@upm.es

Keywords: *Wind Turbine Blade, Airfoil Catalogue, Turbulence Models, CFD, OpenFOAM, Wind Tunnel Test*

Abstract

A methodology to efficiently simulate wind tunnel tests of several airfoils with OpenFOAM has been developed in this work. This methodology bridges OpenFOAM capabilities with Matlab postprocessing to analyse efficiently the performance of wind turbine airfoils at any angle of attack. This technique has been developed to reduce the cost, in terms of time and resources, of wind tunnel campaigns on wind turbine blade airfoils. Different turbulence models were used to study the behaviour of the airfoils near stall.

Wind turbine airfoils need to be characterized for all possible angles of attack, in order to reproduce the real aerodynamic patterns during operation. Unfortunately, this situation is translated into a huge demand of wind tunnel testing resources, airfoil manufacturing and data post-processing. The high costs in terms of experimental measurements have encouraged many researches to elaborate airfoil catalogues by performing CFD simulations.

Results are compared with a testing campaign on wind turbine airfoils aerodynamics run at AB6 wind tunnel of IDR/UPM located at the campus Universidad Politécnica de Madrid (Madrid, Spain), this tunnel being particularly suited for bi-dimensional applications. It is an open wind tunnel with a test section of 2.5 x 0.5 m, the turbulence intensity is under 3% at a Reynolds number of Re $\cong 5 \times 10^5$. The central part of the airfoil mock-ups were built with a 3D printer Additive Fused Deposition Modelling technology (FDM). Simulation results show a fair agreement with experiments, and helped to improve the performance of the wind tunnel.

Introduction

Wind turbine airfoils need to be characterized for all possible angles of attack, in order to reproduce aerodynamic behaviour from any real operating condition. Unfortunately, this requires a huge demand of wind tunnel testing resources, airfoil manufacturing and data post-processing. The high costs in terms of experimental measurements has inspired this work to elaborate an airfoil catalogue by performing CFD simulations with the open source CFD software OpenFOAM, following the example of existing researches [1, 2]. Although most of them only analysed the performance at angles of attack in the range of $-20°$ to $20°$, some interesting works studying the airfoil performances at very high angles of attack can be found in the literature; see for example the report [3].

In [1] the design and experimental verification of RisØ-B1 airfoil family using a structured mesh is presented. A direct design method based on an optimization algorithm coupled with XFOIL is presented. Transition was modelled by the e^n method. *Ellipsys* code was used to verify the magnitude of $C_{l,max}$ and the shape of C_l in the post stall region. Leading edge roughness, stall strips, vortex generators and Gurney flaps are studied at Reynolds number Re $\in \left[1.6 \times 10^6, 9 \times 10^6\right]$. The combination of Gurney flaps and vortex generators was shown as an attractive option for the root of a wind turbine blade.

Numerical simulations can help understand the airfoil aerodynamics, reduce the number of models to be manufactured and tested, and also improve the quality and reliability of the wind tunnel testing, for example by improving the pressure taps distribution on the models surface to measure the wind flow effects.

An efficient meshing technique to simulate two-dimensional flow field around a generic body was created and validated through the prediction of the performance of the NACA 0012 airfoil. This methodology, indeed, allows to generate the mesh for only one incidence, and simply modify it to obtain the mesh for other angles of attack without the need of creating a new mesh from the beginning, resulting in a considerable reduction of the overall computational time.

In this work, the post-stall behaviour of airfoils is not studied due to the extremely high computational cost of unsteady numerical simulations.

Experimental Set Up

The AB6 is an open wind tunnel with a test section of 2.5 x 0.5 m and a length 4 m, with a contraction upstream of 4.5:1 . The turbulence intensity is under 3% for a flow speed of 25 m/s at the center of the test section, the Reynolds number is around $Re \cong 5 \times 10^5$. The airfoils chord is 0.3 m and the span 0.49 m, the maximum blockage of the test section is between 3% at small angles of attack, up to 12% at 90°. Airfoil was mounted at 1.225 m from the tunnel floor and at 1.9 m from the nozzle outlet. A sketch of the wind tunnel is shown in Figure 1.

Pressure measurements were carried out at the central section of the airfoil surface using pressure taps. The airfoil pressure distribution was integrated to obtain normal force, lift and drag and moment coefficients. The airfoil section was equipped with 53 to 63 pressure taps depending on the airfoil, having a diameter of 1.5 mm.

The pressure differential model ZOC 33/64PxX2 from Scanivalve Corp and a positioner Newport model RV- 120-PPHL with a precision of 1/1000 degree were used. LabView interface was used to control positioner, data acquisition system, pressure probes and ambient conditions. Pressure was measured for 35 seconds with a sampling frequency of 150 Hz. Figure 2 shows the test chamber.

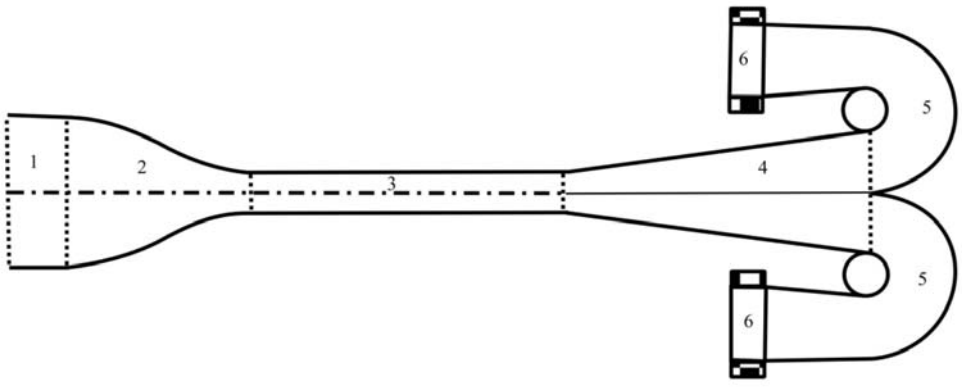

Figure 1: Wind tunnel sketch: 1) grid; 2) contraction; 3) test section; 4) nozzle; 5) elbow; 6) fan.

(a) Intake detail.

(b) Airfoil placed in the test chamber.

Figure 2: Details of UPM AB6 wind tunnel.

Numerical set-up

The software chosen for this study is the open source CFD software OpenFOAM. The solver used is *simpleFoam*, a steady-state solver for incompressible, viscous and turbulent flow based on the SIMPLE algorithm.

Different turbulence models and different near-wall treatments have been used. With wall functions, high-Reynolds turbulence models ($\mathrm{Re} \cong 6 \times 10^6$), namely k-ω SST, k-ε , realisable k-ε and Spalart-Allmaras were simulated. When resolving boundary layer, low-Reynolds turbulence models ($\mathrm{Re} \cong 2 \times 10^5$ and $\mathrm{Re} \cong 5 \times 10^5$), namely Launder-Sharma k-ε, k-ω SST and Spalart-Allmaras. A different mesh is used for $\mathrm{Low-Re}$ problems, trying to keep $y^+ < 1$. Also, a simple grid independence analysis was performed using the k-ω SST model and taking advantage of the refineWallLayer utility, using the drag coefficient C_d at zero incidence as parameter. The characteristics of the different meshes and the results are presented in Table 1.

The *Mesh 1* described in Table 1 was chosen for the simulations, to reduce computational costs in terms of time and resources, since the error with respect to the finest mesh used can be considered sufficiently low. The final mesh is displayed in Figure 3.

The numerical schemes have been chosen, according to mesh quality, following instructions and suggestions provided in [4]. All the schemes are collected in the Table 2, referred to using OpenFOAM's syntax.

The boundary condition used at the inlet and outlet is *freestream* (for pressure *freestreamPressure*) and *calculated uniform 0* for ν_T. For ε *fixedValue* at the inlet and *zeroGradient* at the outlet. On the airfoil surface no slip for velocity and *zeroGradient* for pressure, wall functions are used with high-Reynolds and for low-Reynolds a small *fixedValue* (1×10^{-12}) was used. For more details about the boundary conditions see [5].

Meshing technique

Often, when simulating flows around a body at different angles of attack, a new mesh is generated for each angle of attack. It is easy to understand how this makes the pre-processing phase very time-consuming. A solution could be using an O-mesh or a C-mesh and changing the inlet boundary condition for the velocity, but this cannot be done when simulating a real wind tunnel.

In this work, OpenFOAM native mesh generators, *blockMesh* and *snappyHexMesh,* and its utilities were used to generate, rotate and merge the several meshes used to simulate the flow around the studied airfoils at different angles of attack. Basically, the body is surrounded by a cylindrical region that can be split from the rest of the mesh, rotated to change the angle of attack, and then stitched again to the external region. The procedure relies on the following OpenFOAM utilities:

- *blockMesh* to generate a background, structured mesh.
- *surfaceFeatureExtract* to create a file containing information about the geometry.
- *snappyHexMesh* to generate the mesh around the body.
- *topoSet* to generate two files containing a list of the cells of the internal and external region.

- *splitMeshRegions* to split the two regions of the mesh.
- *transformPoints* to rotate the inner mesh .
- *mergeMeshes* to merge again the two meshes.
- *stitchMesh* to stitch the mesh, deleting the existing internal patches.
- *extrudeMesh* to make the mesh suitable for 2D applications.

The strategy of splitting and rotating the internal mesh (see Figure 3) allows to conduct the simulations reducing strongly the required computational time to generate the new meshes. This strategy could also be use to interpolate between the wind tunnel test results if problems arise in the measurement process. This methodology makes the process of simulating the flow around a body independent of the shape of the body after a few iterations to find the right parameters for *snappyHexMesh*. For more details about the meshing technique see [5].

Table 1: Mesh independence analysis for grid convergence: parameters from the snappyHexMeshDict dictionaries of the different meshes studied; drag coefficient and percentage difference on the prediction of the drag coefficient with respect to *Mesh 1* results as functions of average yplus

	refinementSurfaces	layers	expansionRatio	finalLayerThickness
Mesh 1	level(3 4)	nLayers 10	1.15	0.3
Mesh 2	level(3 4)	nLayers 15	1.15	0.3
Mesh 3	level(4 5)	nLayers 20	1.15	0.3
Mesh 4	Mesh 3 + *refineWallLayer* ('airfoil') 0.435			
	y^+_{avg}	C_d (DC)	$\frac{C_\mathrm{d} - C_{\mathrm{d}_1}}{C_\mathrm{d}} \times 100$	
Mesh 1	1.02	132.60	0.0	
Mesh 2	0.577	136.67	3.0	
Mesh 3	0.152	139.45	4.9	
Mesh 4	0.0649	139.51	4.9	

Table 2: Numerical schemes, OpenFOAM CFD simulation

ddtSchemes	**gradSchemes**
default	default
steadyState	cellMDLimited Gauss linear 0.5
divSchemes	
default	div((nuEff*dev2(T(grad(U)))))
Gauss linearUpwind	Gauss linear
laplacianSchemes	**interpolationSchemes**
default	default
Gauss linear limited 1.0	linear
snGradSchemes	**wallDist**
default	method
limited 1.0	meshWave

Results

Validation

An example of the mesh generated with the above-mentioned procedure around the NACA 0012 airfoil is shown in Figure 3.

Different turbulence models were used in order to reproduce flow detachment and stall conditions. Besides, the effects of the Reynolds number, varying it from $\mathrm{Re} = 2 \times 10^5 - 6 \times 10^6$, were analyzed with RANS simulations using *realizable* k-ε, k-ω *SST* and *Spalart–Allmaras* turbulence models. The simulations have been performed in the linear region of the lift coefficient c_l up to stall.

High-Reynolds models

Pressure distributions and polar diagrams obtained from the different airfoils studied are successfully compared to the corresponding ones from the available literature [6, 7, 8, 9], obtained with wind tunnel testing and numerical simulations. The example provided in Figure 4 refers to the validation case of the performances of NACA 0012 airfoil, using the above-mentioned turbulence models, at $Re = 6 \times 10^6$. The Reynolds number chosen is the same of the references [9, 8], whose results are used as terms for comparison together with results obtained with XFOIL [10]. It is clear that the lift and drag coefficients are very close to the ones from literature for low angles of attack, and less accurate when approaching the stall due to an early prediction of flow detachment.

Low-Reynolds models

The lift and drag coefficients have been calculated and compared with results from a Master thesis project [11] developed at the Technical University of Denmark, obtained in OpenFOAM using a structured mesh and the k-ω SST turbulence model at $Re = 2 \times 10^5$, and results obtained with XFOIL at the same Reynolds number. They are shown in figure 5.

A difference of slope in the linear part of the curve between the predictions obtained with the structured and the hybrid mesh can be observed. Also the simulation with the hybrid mesh predicts the stall at a clearly lower incidence. The e^n method was used in XFOIL with $n = 9$. The simulations from [11] overestimated stall predicting a much higher maximum lift coefficient.

Results: airfoil catalogue

The geometries studied in the catalogue are shown in Figure 6. For each studied airfoil the lift and drag coefficient as well as pressure coefficient at 6° and 12° of angle of attack are presented in this section.

NACA 63_2A015

This airfoil is a modified version, identified with the capital letter "A", of the corresponding NACA 6-series airfoil. These airfoils were designed to maximise the chordwise extent of laminar flow in order to reduce the drag coefficient, at least in a limited range of operating conditions close to the design lift coefficient [12]. Thus their polar are characterised by a region of lower drag, with centre at the design lift coefficient, known as low-drag bucket.

The NACA 63_2A015 is a symmetric airfoil, whose thickness is the 15% of the chord, the design coefficient is equal to zero and the extent of the low-drag bucket is 0.2 above and below the design lift coefficient.

Generally speaking, experimental data are not in good agreement neither with XFOIL nor with computational simulations. The zero-lift angle is not zero, even though the airfoil is symmetric; the slope of the lift curve is underestimated, while the angle of maximum lift, the maximum lift coefficient and the minimum drag coefficient are close to the other predictions.

Concerning the lift coefficient, the first two turbulence models give very close results, which also are in great agreement with data from XFOIL; slight differences can be appreciated in the stall region, whereas the maximum lift coefficient an the incidence of maximum lift are still very close.

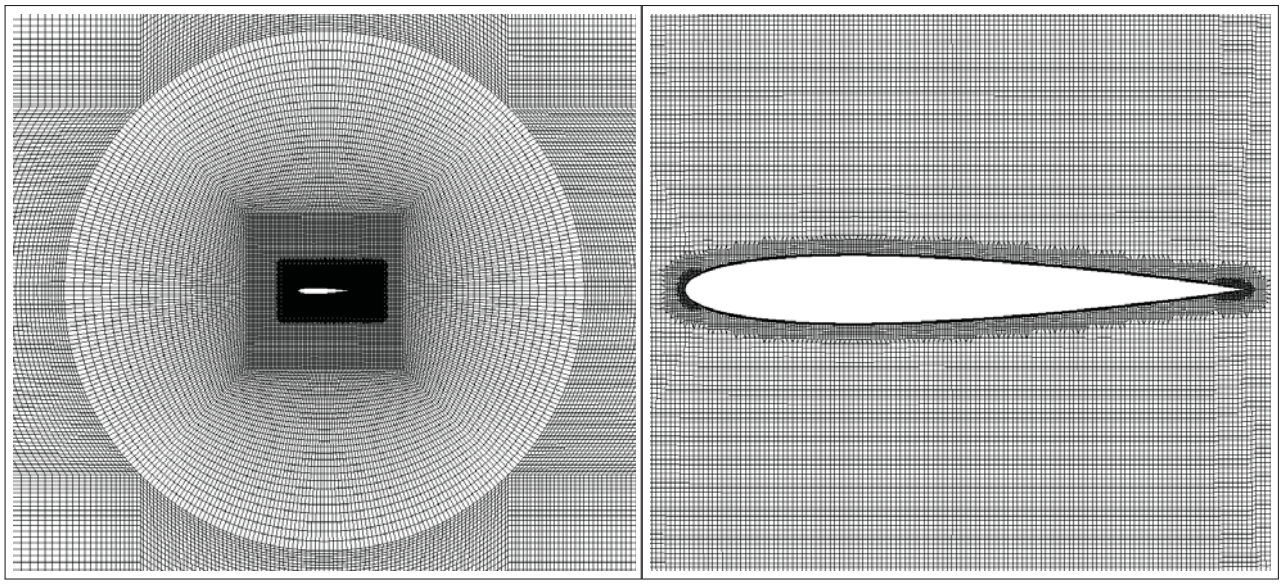

(a) Mesh structure. (b) Detail of the mesh around the airfoil.

Figure 3: Mesh around NACA 0012, snappyHexMesh mesh generator.

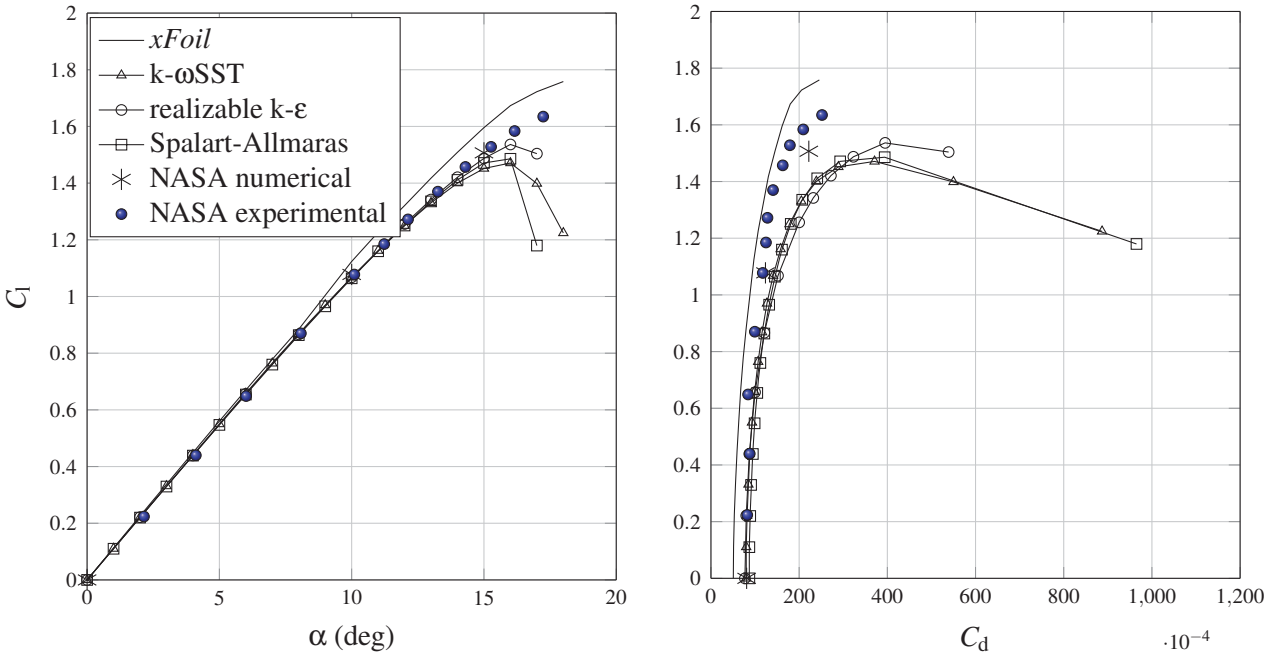

(a) Lift curve. (b) Drag polar.

Figure 4: NACA 0012 performance, comparison among different turbulence models, $\mathrm{Re} = 6 \times 10^6$**.**

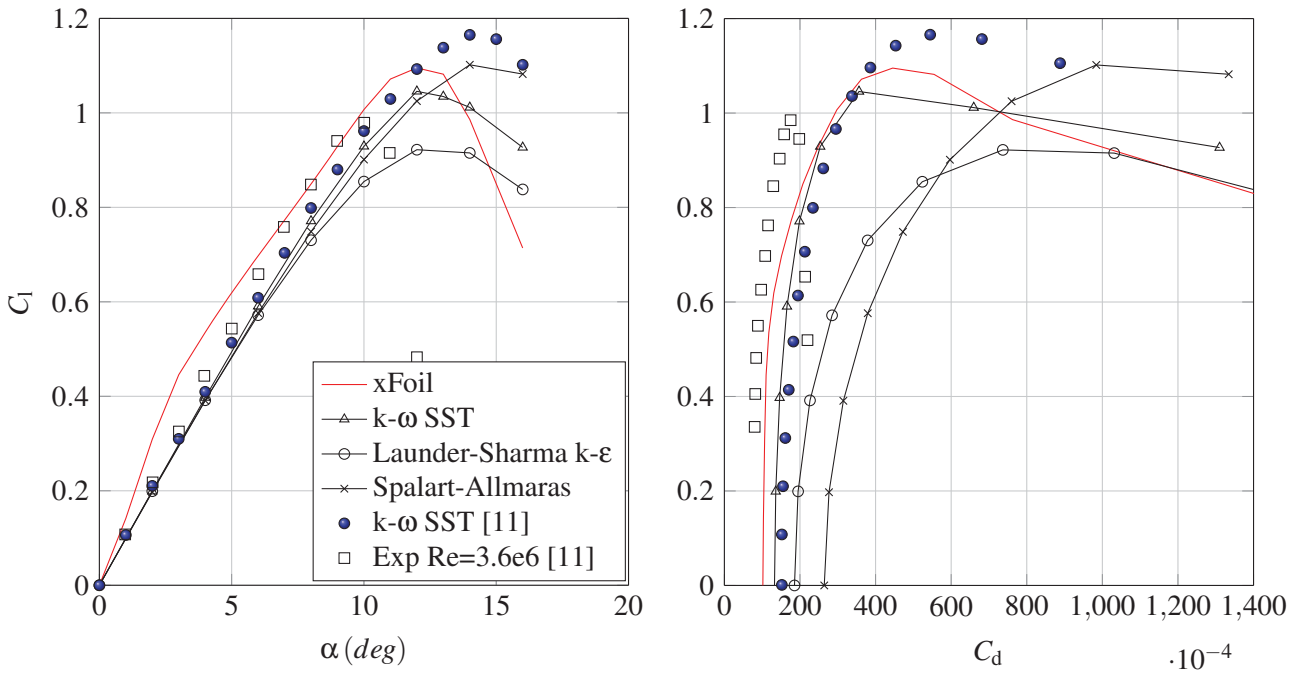

(a) Lift curve

(b) Drag polar

Figure 5: Performance of the NACA 0012, $Re = 2 \times 10^5$, OpenFOAM CFD simulation, comparison among predictions with different low-*Re* turbulence models

The prediction of the curve's slope in the linear region obtained with the Launder-Sharma k-ε turbulence model is in fair agreement with XFOIL and the ones obtained with the other turbulence models; the maximum lift coefficient is underpredicted, even though the angle of maximum lift is very close to the other results.

All the turbulence models predict higher drag coefficients than XFOIL.

DU 91-W2-250

The DU 91-W2-250 is the first of the three wind turbine dedicated airfoils designed at the Technological University of Delft included in the catalogue. More information and data can be found in [13, 14]. As the designation suggests it, has a thickness equal to the 25% of the chord, being suitable as airfoil for mid sections of wind turbines' blades [13].

Lift and drag coefficients obtained with the k-ω SST and Spalart-Allmaras turbulence models in OpenFOAM are compared with XFOIL calculations and experimental data as shown in Figure 8 and 9.

Regarding the lift coefficient, results from computational calculations are in good agreement, except in the stall region at negative incidences. The predictions of the lift curve slope are in between experimental data and XFOIL calculations. Experimental data show a considerable improvement after the implementation of wind tunnel corrections (CB). Among the correction performed in the wind tunnel an adhesive foam was place between the airfoil and the tunnel walls reducing leakage and Pitot tube was relocated.

Concerning the drag coefficient, both computational predictions of the minimum drag coefficient overestimate XFOIL and experimental data, but the variation of the drag coefficients as function of the lift coefficient are quite similar to XFOIL. Experimental minimum drag coefficient is very close to XFOIL calculation, and again the correction have improved the results. At high angles of attack the differences in drag coefficient are higher.

Despite the differences between test and simulations in pressure coefficient distribution around the airfoil are reduced after tunnel corrections, the increase with the angle of attack of this differences in the pressure side in the rear part of the airfoil leads to think that a small leakage could still remain.

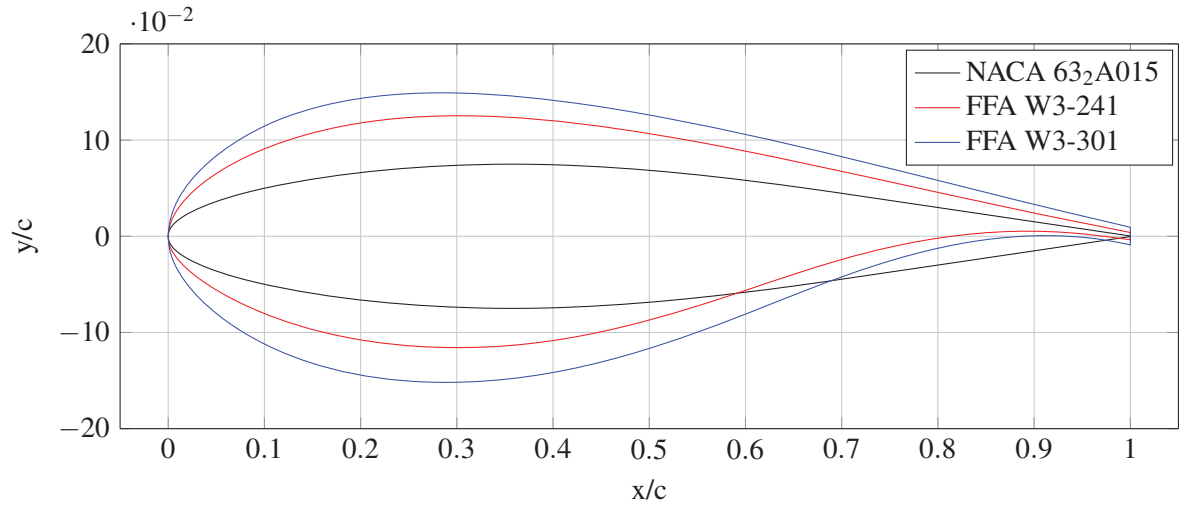

(a)

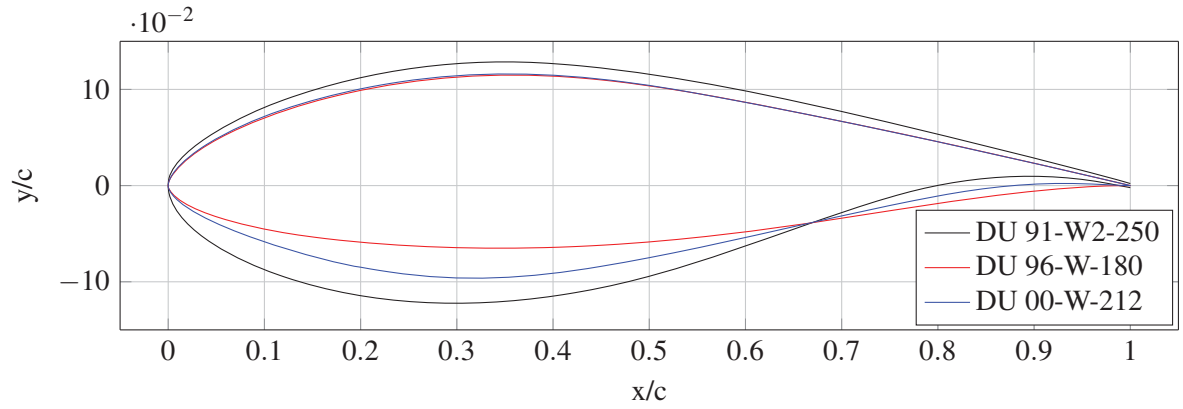

(b)

Figure 6: Wind turbine airfoil geometries.

DU 96-W-180

This is the second airfoil from the DU series analysed. The thickness of the DU 96-W-180 is the 18% of the chord, and is thus suitable for the tip sections of wind turbines' blades [13]. The lift coefficient, predictions obtained with both turbulence models are very close to XFOIL results except for the stall region. Indeed, the slopes of the lift curves and the zero-lift incidences are in good agreement, whereas the maximum lift coefficients obtained from CFD calculations are lower than XFOIL prediction. Nevertheless, the maximum lift incidence and the post-stall behaviour are predicted very accurately with the k-ω SST turbulence model.

The predictions of the drag coefficient, as for all the other cases studied, are higher than XFOIL results, whereas the behaviour of the drag coefficient, which change very little until massive separation occurs, is qualitatively similar.

In airfoil DU 96-W-180 a bump is shown in the pressure coefficient on the suction side (see Figure 12) at $x = 0.35c$, it extends to $x = 0.45c$

The recirculation bubble and other instabilities that arise in the low Reynolds number flow can not be captured without transition turbulence models.

DU 00-W-212

This is the third and last airfoil from the DU series. The thickness of the DU 00-W-212 is around the 21% of the chord, and is thus suitable for the mid sections of wind turbines' blades [13].

Regarding the lift coefficient, results obtained in OpenFOAM and experimental ones are in great agreement at positive incidence, but are very different at negative incidence. XFOIL calculations show higher slope and maximum lift coefficient. The post-stall behaviour is qualitatively similar for XFOIL calculations, OpenFOAM

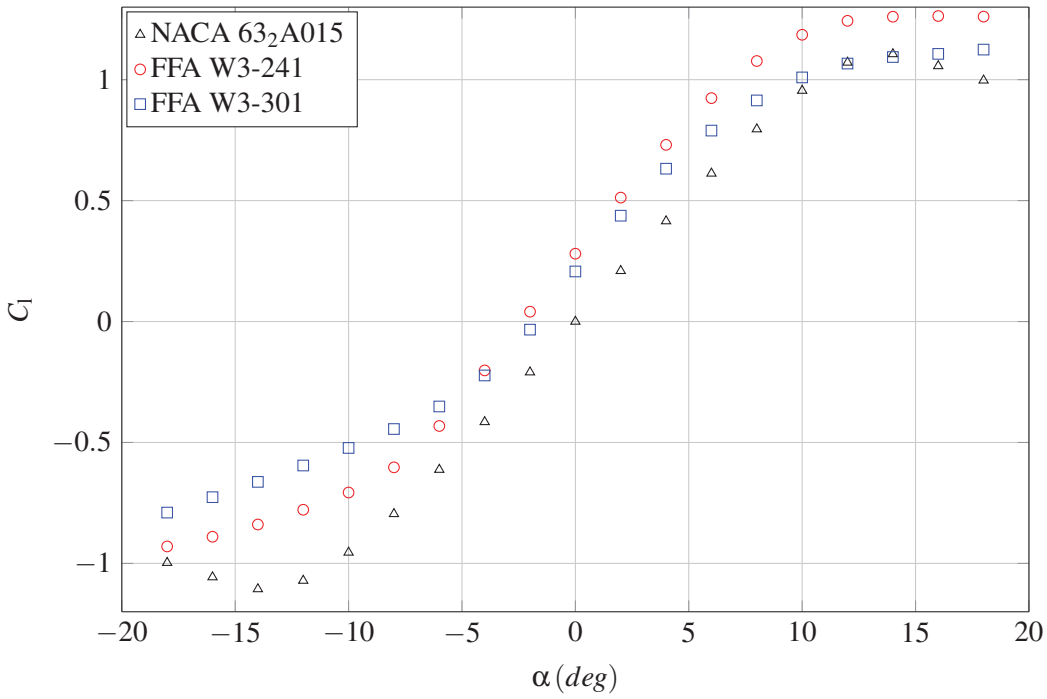

(a) Lift curve

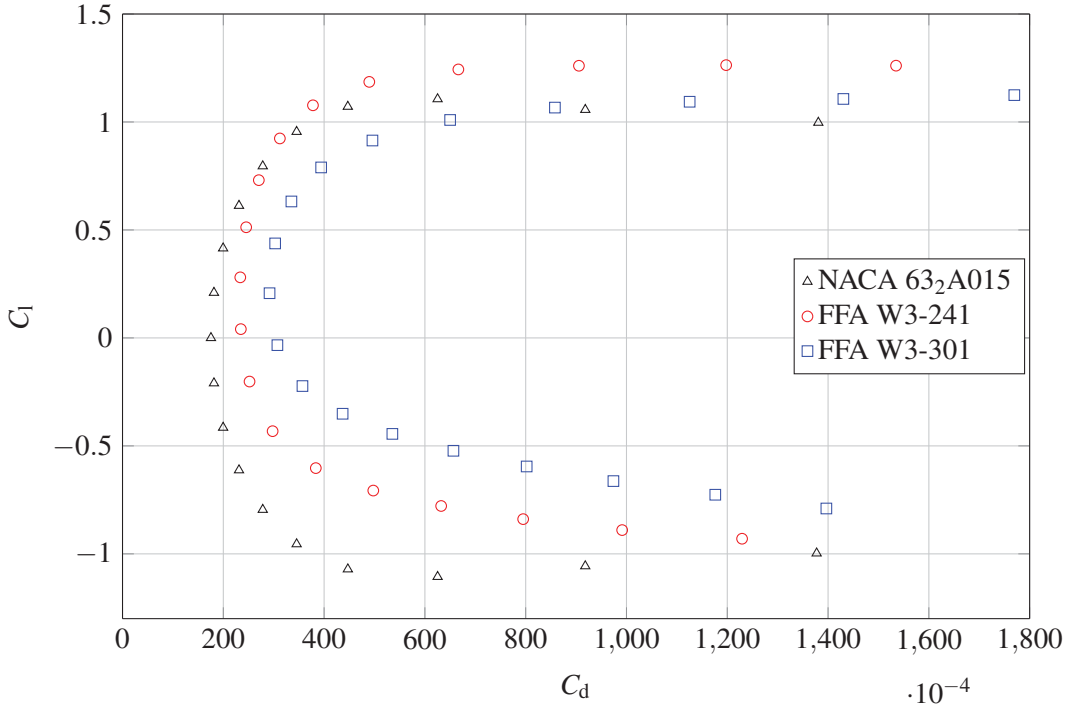

(b) Drag polar

Figure 7: Performance FFA NACA

predictions with k-ω SST model and experimental data, with a slight decrease of the lift coefficient as the angle of attack increases. The maximum lift coefficient is similar for each curve except the one obtained with the k-ω SST turbulence model.

The drag coefficient curves obtained with OpenFOAM and XFOIL are qualitatively similar, but OpenFOAM predicts higher drag. The minimum drag coefficient from experimental data is in good agreement with XFOIL results, but increases far more rapidly as the incidence increases.

FFA W3-241

This is one of two airfoils designed at the Aeronautical Research Institute of Sweden (FFA) included in this catalogue. More information and data about this family can be found in [6].
The FFA W3-241 thickness, as highlighted in the designation, is the 24% of the chord.

The results obtained are considerably different, especially the lift coefficients.

The lift coefficients predicted with the two turbulence models are very similar and intermediate between XFOIL and experimental results at positive angles of attack, whereas they start differing and are lower than both XFOIL and experimental data at the lowest angles of attack.

Also in this case the drag coefficients obtained in OpenFOAM are qualitatively similar to and higher than XFOIL ones. Again, the minimum drag coefficient from experimental tests is very close to XFOIL calculation.

FFA W3-301

This is the second and last airfoil of the FFA series to be studied. The FFA W3-301's thickness is around the 30% of the chord as shown in Figure 6.

Lift and drag coefficients obtained with the Spalart-Allmaras turbulence models in OpenFOAM are compared together with FFA W3-241 and NACA 63_2A015 in Figure 7.

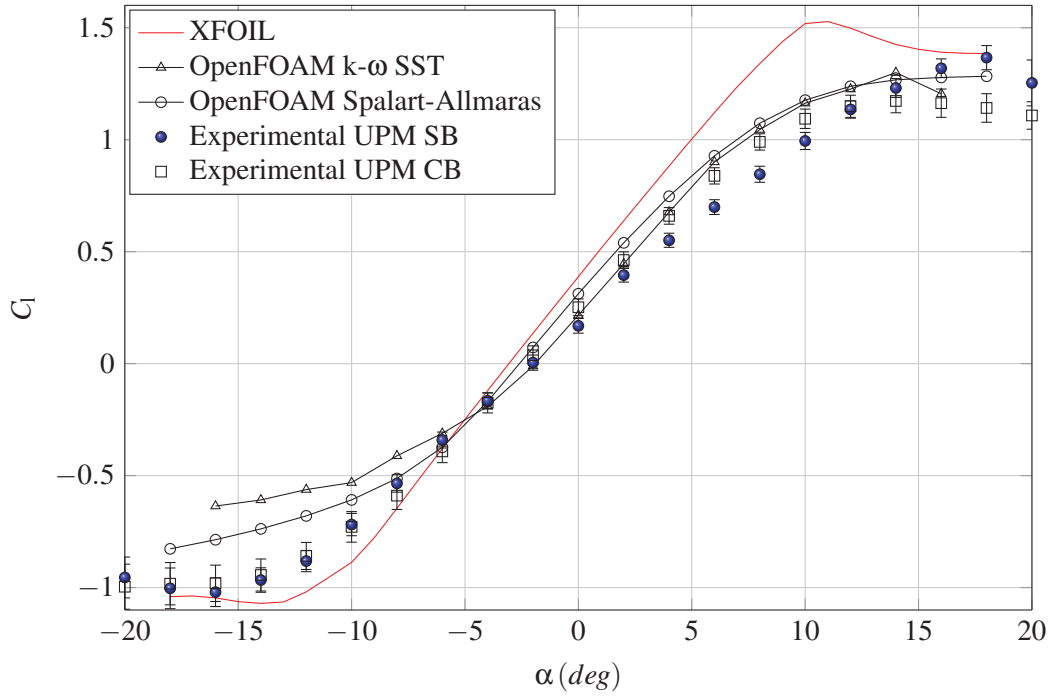

(a) Lift curve.

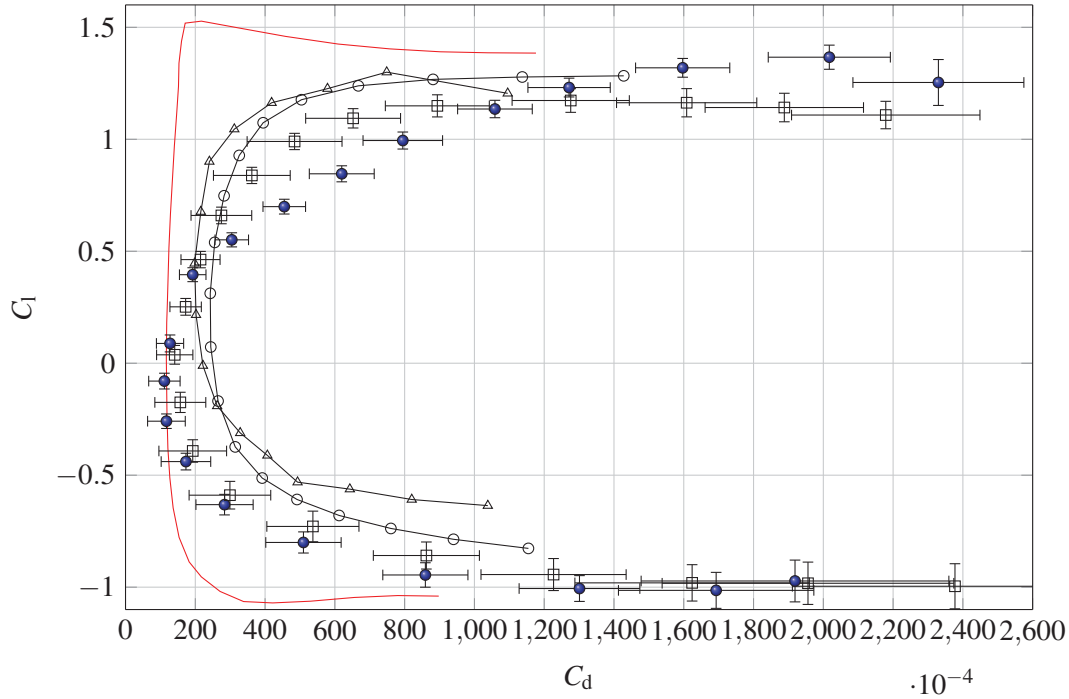

(b) Drag polar.

Figure 8: Performance of the DU 91 W2-250, $Re = 5 \times 10^5$, comparison between numerical results from OpenFOAM CFD simulation with different turbulence models, results from experimental tests performed at UPM and results from XFOIL

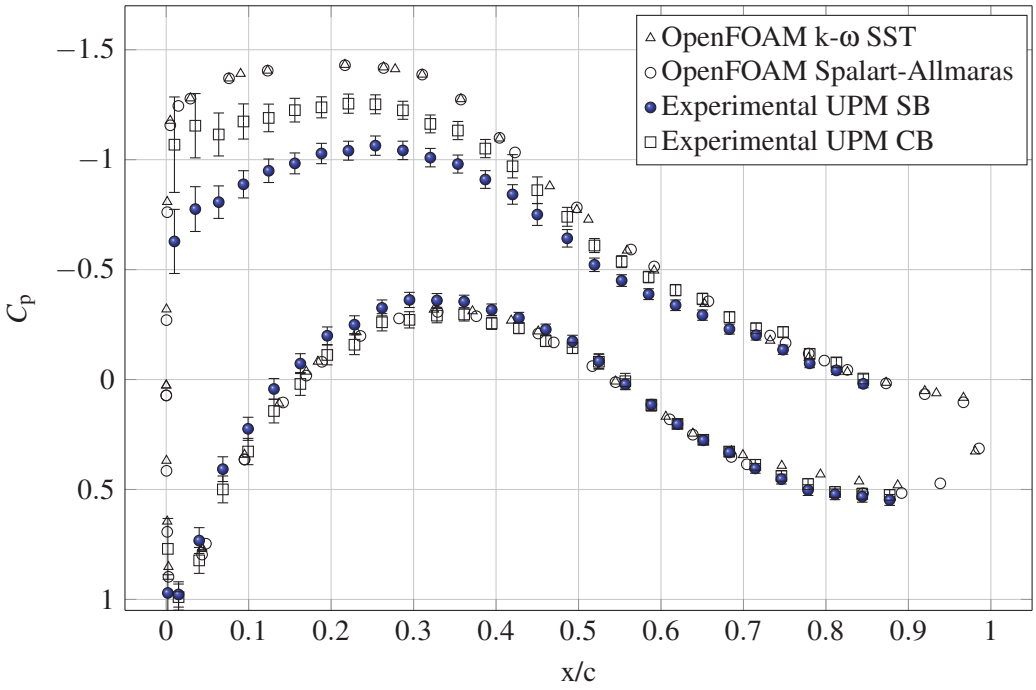

(a) $\alpha = 6^\circ$

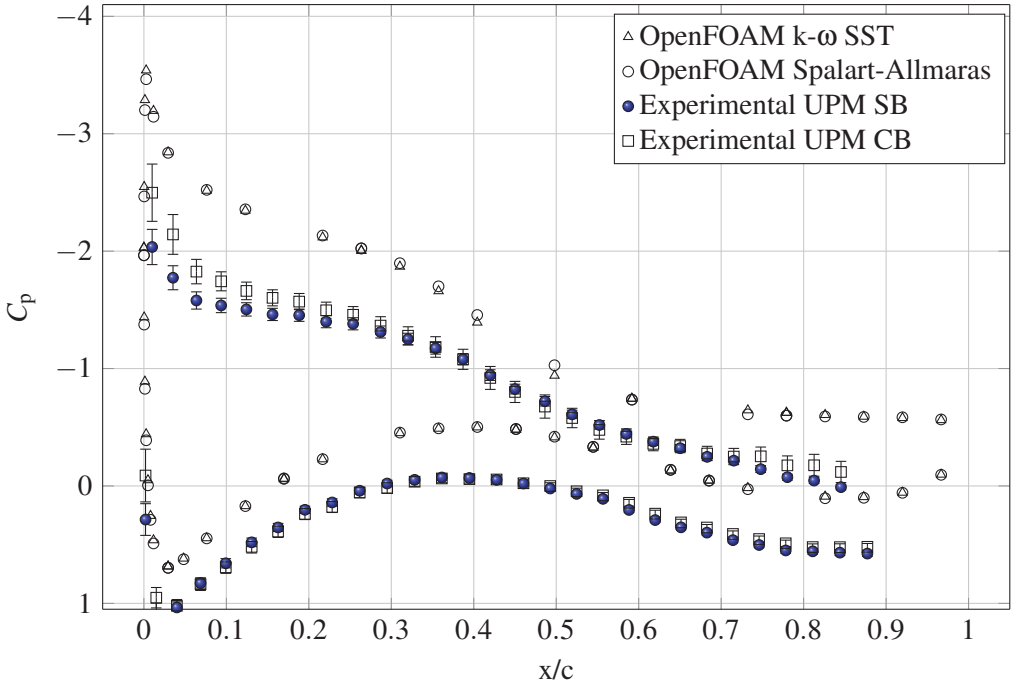

(b) $\alpha = 12^\circ$

Figure 9: Distribution of pressure coefficient along the chord of the DU 91 W2-250, $Re = 5 \times 10^5$, comparison between numerical results from OpenFOAM CFD simulations with different turbulence models and results from experimental tests performed at UPM

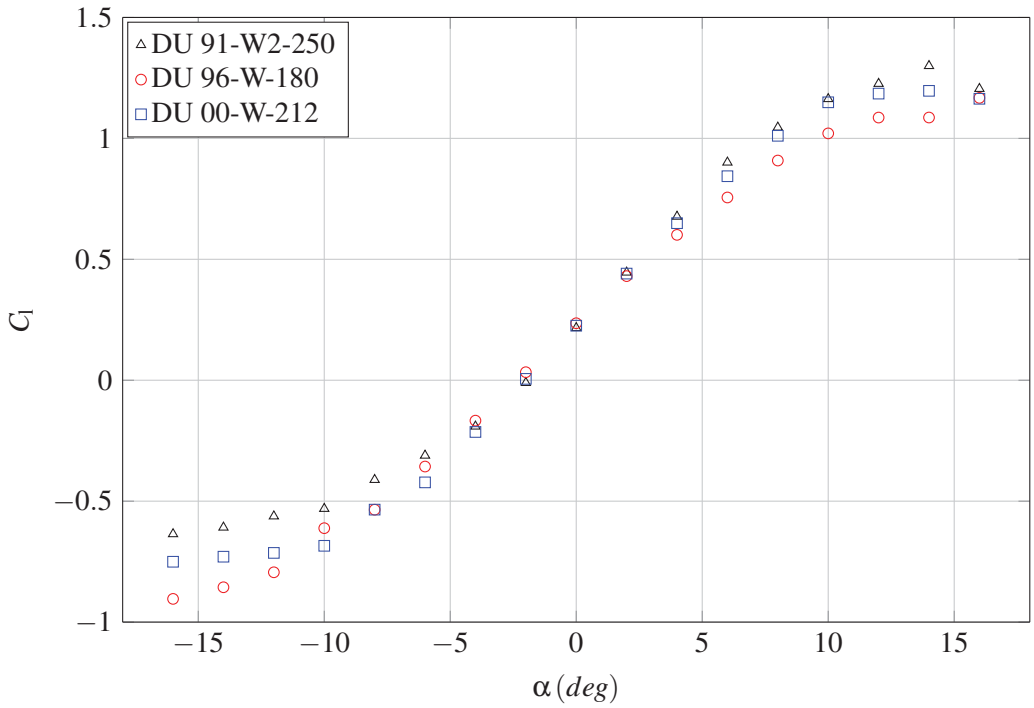

(a) Lift curve.

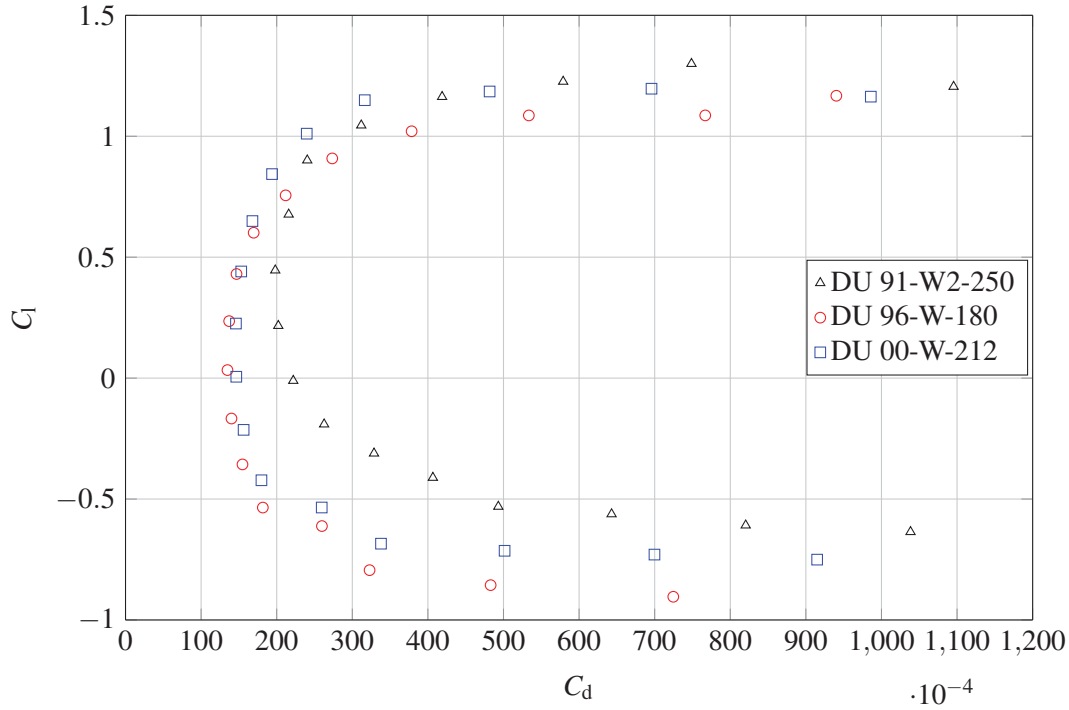

(b) Drag polar.

Figure 10: Performance DU

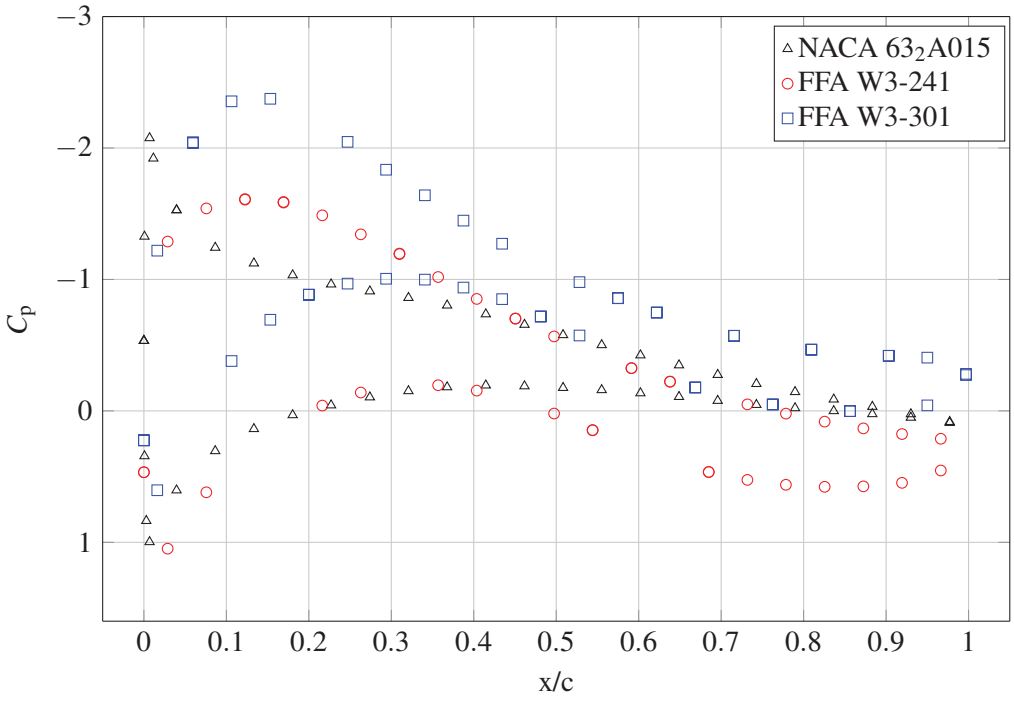

(a) $\alpha = 6°$

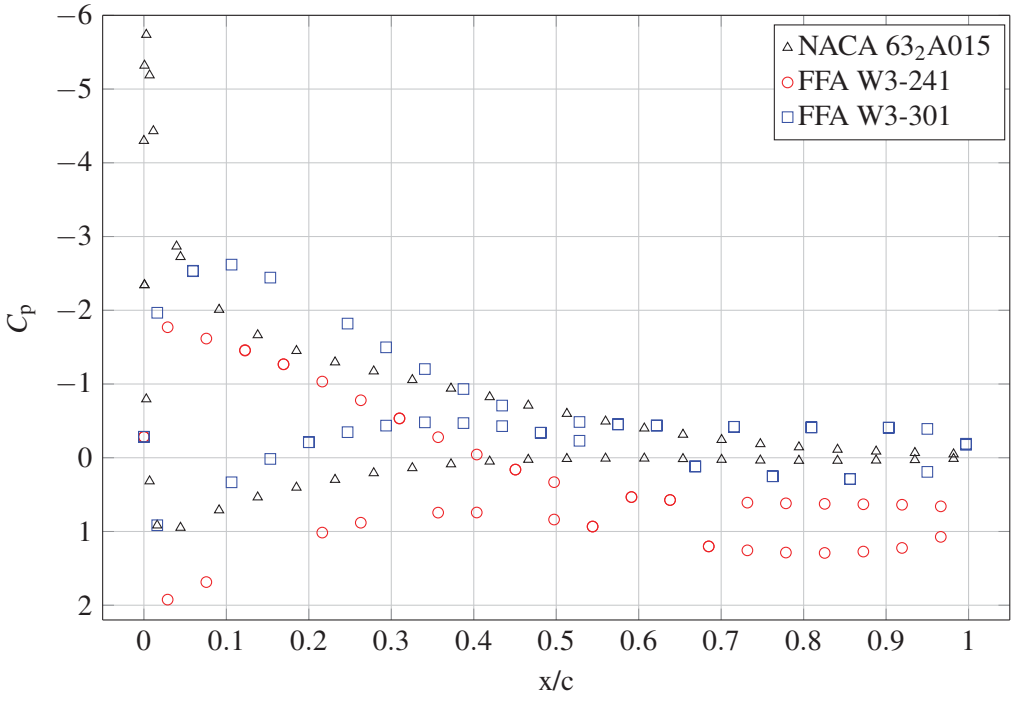

(b) $\alpha = 12°$

Figure 11: Distribution of pressure coefficient along the chord for FFA and NACA

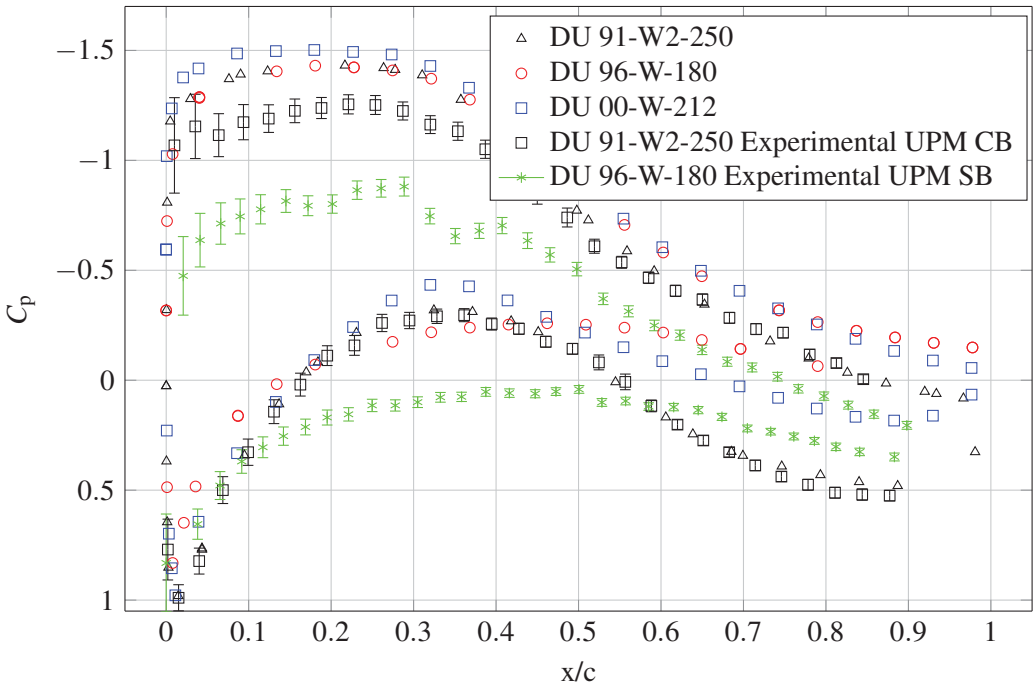

(a) $\alpha = 6°$

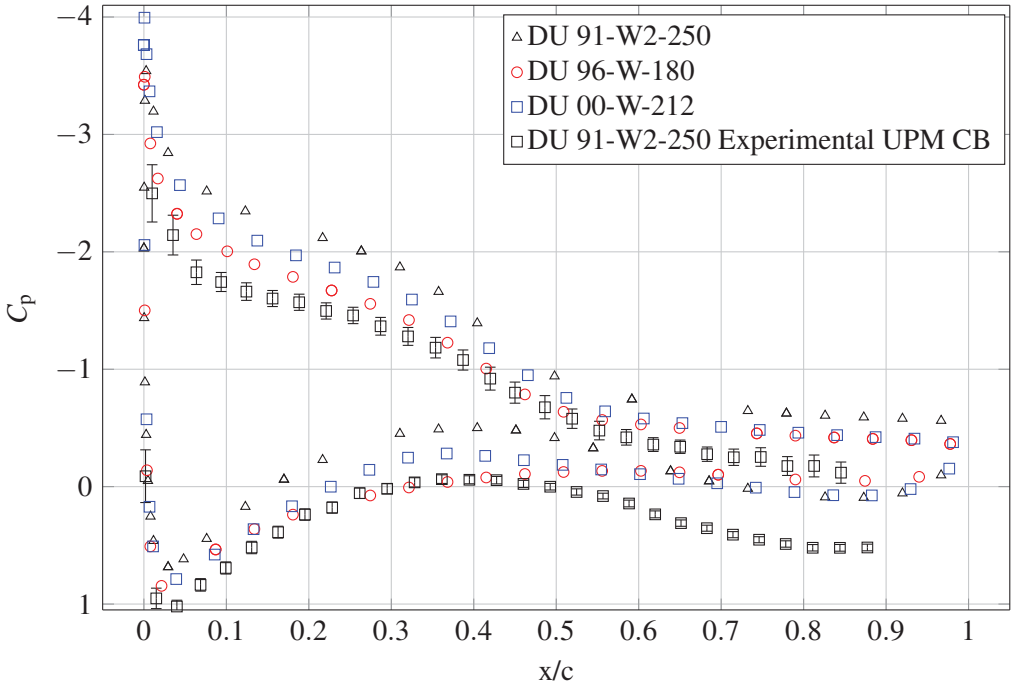

(b) $\alpha = 12°$

Figure 12: Distribution of pressure coefficient along the chord for DU family at $\alpha = 6°$ and $\alpha = 12°$

Conclusions

An efficient meshing technique to simulate wind tunnel tests over a generic body for any angle of attack with OpenFOAM has been introduced and successfully validated through a simple test case.

Different airfoil families used on wind turbines have been simulated with the proposed methodology.

OpenFOAM simulations help to understand the aerodynamics of wind turbine airfoils, to reduce the number of models to be manufactured and tested, and also to improve the quality and reliability of the wind tunnel facility (i.e., improving the pressure taps distribution on the models surface to measure the wind flow effects, leakage detection, etc).

Simulation results with high and low Reynolds turbulence models have been compared with experimental results, XFOIL and other simulations found in the bibliography.

The low Reynolds turbulence model simulations did not capture the recirculation bubble in the suction side. This highlights the importance of using transitional models in order to reproduce accurately the flow field around the airfoil.

References

[1] Peter Fuglsang, Christian Bak, Mac Gaunaa, and Ioannis Antoniou. Design and verification of the riso-b1 airfoil family for wind turbines. In *42nd AIAA Aerospace Sciences Meeting and Exhibit*, page 668, 2004.

[2] Franck Bertagnolio, Niels N. Sørensen, Jeppe Johansen, and P. Fuglsang. Wind turbine airfoil catalogue. Technical report, Technical University of Denmark, 2001.

[3] M. L. Shur, P. R. Spalart, M. Strelets, and A. Travin. Detatched-eddy simulation of an airfoil at high angle of attack. *Engineering turbulence modelling and experiments*, 4:669–678, 1999.

[4] J. Guerrero. Introductory openfoam course-training, module 9. *University of Genoa, Dipartimento di Ingegneria Civile, Chimica e Ambientale (DICCA)*, 2016.

[5] Lorenzo Donisi. 2D Investigation of aerodynamic performance of wind turbine dedicated airfoils with OpenFOAM. Master's thesis, Universidad Politécnica de Madrid, 2017.

[6] Anders Bjorck. Coordinates and calculations for the FFA-WL-XXX, FFA-W2-XXX and FFA-W3-XXX series of airfoils for horizontal axis wind turbines. Technical report, The Aeronautical Research Institute of Sweden, 1990.

[7] S. A. H. Jafari and B. Kosasih. Flow analysis of shrouded small wind turbine with a simple frustum diffuser with computational fluid dynamics simulations. *Journal of Wind Engineering and Industrial Aerodynamics*, 125:102–110, 2014.

[8] C. L. Ladson. Effects of independent variation of mach and reynolds numbers on the low-speed aerodynamic characteristics of the naca 0012 airfoil section nasa-tm-4074,(l-16472, nas 1.15: 4074). *Hampton, VA: National Aeronautics and Space Administration, Langley Research Center*, 1988.

[9] NASA Langley Research Center. Turbulence Modeling Resource. [ONLINE] Available at: https://turbmodels.larc.nasa.gov/index.html. Last Updated 2017.

[10] MIT Mark Drela. Xfoil, subsonic airfoil development system.

[11] T. Kaloyanov. *Investigation of 2D Airfoils equipped with a trailing edge flaps*. PhD thesis, Master Thesis, Technical University of Denmark, Lyngby, Denmark, 2011.

[12] Ira Herbert Abbott and Albert Edward Von Doenhoff. *Theory of wing sections, including a summary of airfoil data*. Courier Corporation, 1959.

[13] Ruud van Rooij and Nando Timmer. Design of airfoils for wind turbine blades. *Delft University of Technology, The Netherlands*, 2004.

[14] W. A. Timmer and R. P. J. O. M. Van Rooij. Summary of the delft university wind turbine dedicated airfoils. In *ASME 2003 Wind Energy Symposium*, pages 11–21. American Society of Mechanical Engineers, 2003.